Can we infer excitation-inhibition balance from the spectrum of population activity?

Kingshuk Chakravarty[1], Sangheeta Roy[1], Aniruddha Sinha[1], Arvind Kumar[2,3]

[1]*Tata Consultancy Services, Kolkata, India*
[2]*Division of Computational Science and Technology,*
School of Electrical Engineering and Computer Science, KTH Royal Institute of Technology Stockholm, Sweden
[3]*Scilife Lab, Stockholm, Sweden*

Abstract

Networks in the brain operate in an excitation-inhibition (EI) balanced state. Altered EI balance underlies aberrant dynamics and impaired information processing. Given its importance, it is crucial to establish non-invasive measures of the EI balances. Previous studies have suggested that relative EI balance can be inferred from the spectrum of the population signals such as Local Field Potentials, Electroencephalogram and Magnetoencephalography. This idea exploits the fact that in most cases excitatory and inhibitory synapses have quite different time constants. However, it is not clear to what extent spectral slope of population activity is related to the network parameters that define the EI balance e.g. excitatory and inhibitory conductance. To address this question we simulated two different types of recurrent networks and measured spectral slope for a wide range of parameters. Our results show that the slope of the spectrum cannot predict the ratio of excitatory and inhibitory synaptic conductance. Only in a small set of simulations a change in the spectral slope was consistent with the corresponding change in the synaptic weights or inputs to the network. Thus, our results show that we should be careful in interpreting the change in the slope of the population activity spectrum.

Significant statement

Non-invasive signals such as electroencephalogram (EEG) and magneto-encephalogram (MEG) are routine acquired from human subjects in different functional and dysfunctional states. It is of great interest to relate properties of EEG/MEG to the underlying physiology and network properties. In this regard, recently it was proposed that the slope of the EEG/MEG spectrum can be related to excitation-inhibition balance: steeper slopes indicate higher inhibition. Here we show that such an explanation holds only for a small set of conditions. In most cases spectral slope is not informative of underlying excitation-inhibition balance. Thus, we argue that while spectral slope may be a good biomarker of brain state, it is not informative about the underlying excitation-inhibition balance or network parameters.

Introduction

Excitation-inhibition (EI) balance has emerged as an important parameter that determines not only the stability of the network [1, 2, 3] but also the statistics of neuronal activity [4, 5, 6], and gain of the network [7]. Experimental data have corroborated results of computational models that both timing and magnitude of excitation and inhibition are tightly maintained for brain function [8, 9, 10]. Furthermore, *in vitro* analysis of neuronal connectivity has revealed that EI balance may be severely altered in pathalogical states [see review by Tatti et al. [11]].

These observations have inspired the development of methods to estimate EI-balance non-invasively. In this regard [12] have made significant progress and proposed that the aperiodic component of population activity may be used

Email address: arvkumar@kth.se (Arvind Kumar)

to extract information on changes in the EI balance. In particular, they argued that steeper slope of spectrum of the population activity (LFP/EEG/MEG) is associated with stronger inhibition (Fig. 1). This argument is based on that fact that typically inhibitory synapses are slower than excitatory ones and population activity is largely associated with trans-membrane currents induced by synaptic inputs [13]. The spectral estimate of (relative) EI-balance implicitly assumes that the inputs to the network are both uncorrelated and asynchronous. However, it is well known that given the network connectivity and neuron properties, network activity may be both synchronous and oscillatory and EI-balance itself is a key determinant of the network activity state [2, 3]. Therefore, it is unclear under what conditions we can use the spectral slope to compare EI-balance between two different situations. Essentially, the question arises when and how the spectral slope is related to the network parameters.

To address this question, we simulated network activity under different levels of EI-balance (as determined by synaptic weights and inputs) and measured the slope of population activity spectrum. We considered two different classes of networks: a neocortical network model in which both excitatory and inhibitory populations were mutually connected, and STN-GPe network in which excitatory recurrent connections were absent. Both network models have been extensively studied for their dynamical properties, in particular synchrony and oscillations [1, 2, 3, 14, 15, 16, 17, 18].

We found that only in a few network configurations an increase in the inhibitory synaptic strength was associated with a corresponding increase in the spectral slope. In most cases, an increase in the spectral slope could be due to both an increase or a decrease in strength of inhibitory inputs. In fact, an increase in the inhibition in two networks with similar parameters often resulted in a different effect on the spectral slope. It can be argued EI balance is a network property governed by the activity state and cannot be solely determined by individual neuron and synaptic parameters. Therefore, we checked how a change in the spectral slope was related to the ratio of total excitatory and inhibitory conductance. Even at that level we did not find any clear relationship between the ratio of excitatory and inhibitory conductance and the spectral slope.

Thus, our results suggest that a change in the spectral slope is not a reliable predictor of EI balance in terms of network parameters or synaptic conductance. Therefore, we argue that we do not yet understand the origin of a change in the spectral slope and we should be cautious while interpreting results based on the spectral slope.

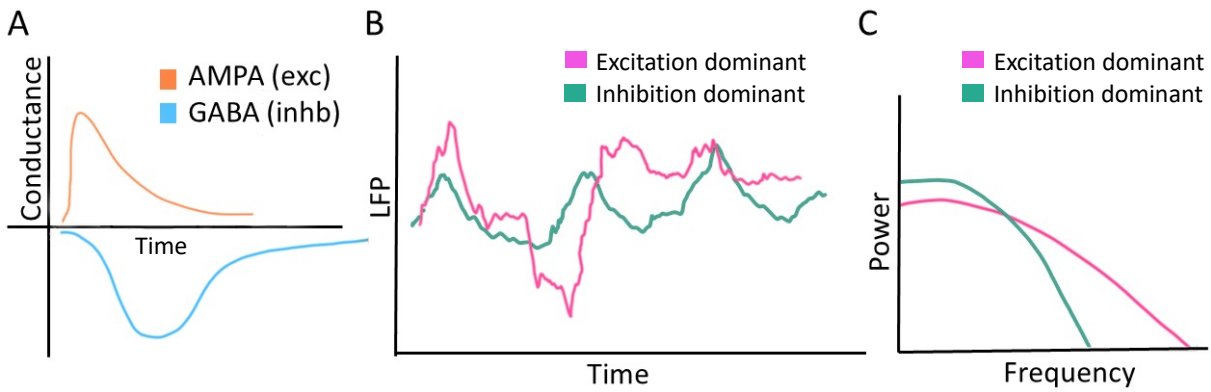

Figure 1: **A schematic diagram to illustrate how excitation and inhibition may influence the power spectrum.** (**A**) Schematic of excitatory and inhibitory postsynaptic conductance. (**B**) Schematic of LFP time series when excitation or inhibition dominates the inputs to a neuron. (**C**) Power spectrum of the LFP shown in panel B.

Methods

Network Structure

STN-GPe network

Here we used a previously published reduced model of the STN-GPe subnetwork of the basal ganglia [16] and modified the inputs and connectivity strengths. Briefly, the network consisted of one excitatory and one inhibitory population which represent the STN and GPe subnuclei of the basal ganglia, respectively(Fig. 2). STN neurons received inhibitory (GABAergic) connections from the GPe, while the GPe received both excitatory (glutamatergic: AMPA) connections from the STN and inhibitory (GABAergic) connections from within the GPe itself. Neurons were connected randomly with a fixed connection probability with conductance-based synapses (see Table 1; for more details please see [16]).

STN and GPe neurons were simulated using leaky integrate-and-fire (LIF) neuron models (see below). Neurons were driven by Poisson-type excitatory spike trains to achieve *in vivo* level of spiking activity. We varied the STN-GPe dynamics by changing following four variables: rate of background inputs to STN and GPe neurons and the strength of synaptic connections STN (i.e. STN→GPe, GPe→STN). To mimic pathological oscillations observed in Parkinson's disease we provided additional inhibitory input (Poisson distributed spike trains) to GPe neurons [15].

Neocortical network

For a model of cortical network we simulated a network of excitatory and inhibitory neurons in which both populations were mutually connected with fixed connection probability [3] (see Table 3). Similar to the STN-GPe model, in the neocortical network model both the excitatory pyramidal (E) and inhibiotry interneurons (I) were modeled using LIF neurons. Deviating from commonly used model we endowed the neurons with different neurotransmitters: excitatory neurons released both AMPA and NMDA while inhibitory neurons released GABA.

Synapse model

To model AMPA and NMDA type synaptic dynamics we used the multi compartment neuronal model (iaf_cond_alpha_mc from NEST simulator v3.8.0). Different ports were assigned to NMDA, AMPA, and GABA receptor, enabling synapses to be categorized based on their input type, i.e., inhibitory GABAergic or excitatory glutamatergic. GABAergic synapses were assigned to the soma, while glutamatergic synapses were connected to the NMDA and AMPA receptor ports. Additionally, the number of inputs targeting NMDA and AMPA receptors was a free variable in our simulation-based analysis (see Table 3).

$$I_{syn} = G_{ion}(V_m - E_{ion}) \tag{1}$$

$$= G_{exc}(V_m - E_{exc}) + G_{inh}(V_m - E_{inh}) \tag{2}$$

$$= G_{\text{AMPA}}(V_m - E_{\text{AMPA}}) + G_{\text{NMDA}}(V_m - E_{\text{NMDA}}) + G_{\text{GABA}}(V_m - E_{\text{GABA}}) \tag{3}$$

Here, G_{AMPA} and G_{NMDA} are the part of excitatory conductance whereas G_{GABA} is the part of inhibitory conductance and E_{GABA}, E_{NMDA} and E_{AMPA} are the reversal potential.

$$G_{type} = g_{max}^{type} \frac{t}{\tau_{type}} \exp(-\frac{t}{\tau_{type}}), \text{ where, type} = \{\text{AMPA, NMDA, GABA}\} \tag{4}$$

g_{max}, (referred to as synaptic weight) is the maximum conductances elicited by each incoming spike.

Neuron model

We used the leaky integrate-and-fire (LIF) model to simulate neurons in the network. The membrane potential (V_m) of a LIF neuron changed over time according to the following equation:

$$C_m \frac{dV_m}{dt} = -g_L(V_m - V_{rest}) + I_{syn} + I_{ext} \tag{5}$$

Where g_L, C_m, I_{ext} are membrane leak conductance, capacitance, external input current to the neuron, respectively. V_{rest} is the resting membrane potential, respectively. $\frac{dV_m}{dt}$ is the rate of change of membrane potential with respect to time. The term I_{syn}represents the sum of all synaptic inputs.

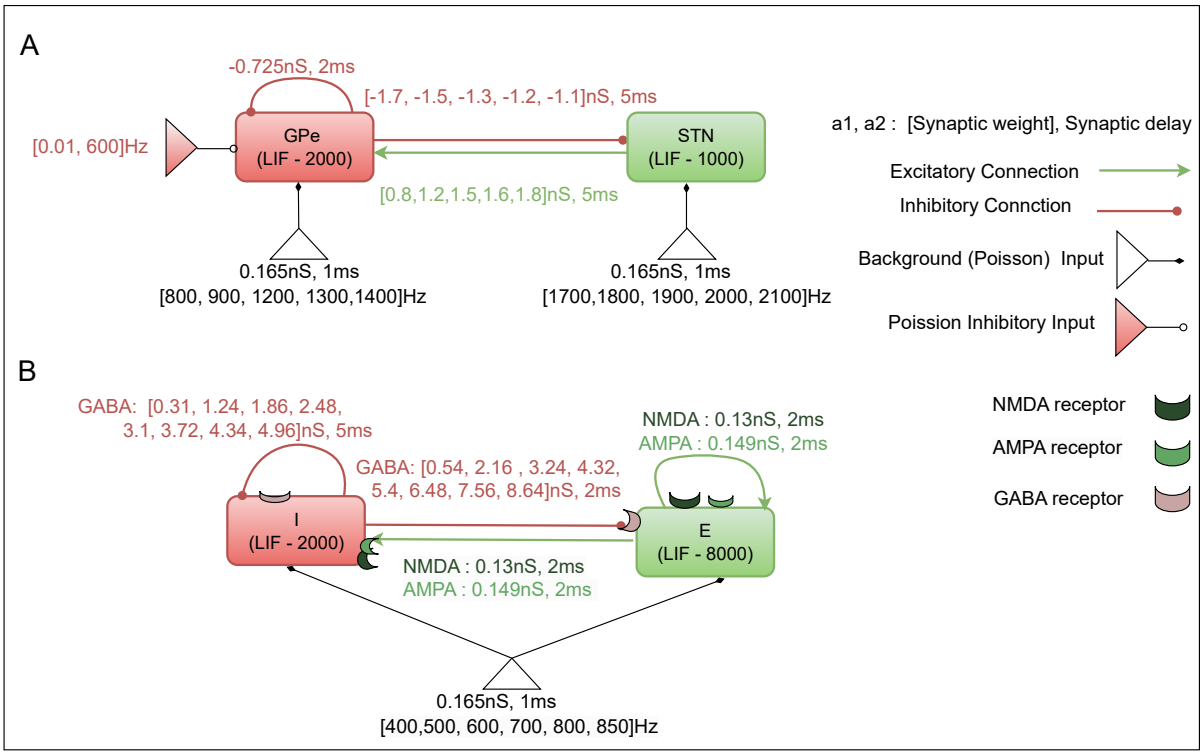

Figure 2: **Schematic diagram of the two networks.** (**A**) STN-GPe network. (**B**) A network with E→E, E→I, I→E and I→I connections. Each neuron in a population (rectangles) received Poisson type excitatory (empty triangles) and inhibitory (filled triangles) spiking input. Strength, synaptic delay and range of input rates of the inputs are written just next to the triangles. Strength and delays of the recurrent connections are written next the relevant connectors (arrows: excitatory and filled circles: inhibitory).

Simulation details

STN↔GPe network: As described in the preceding sections, the STN-GPe loop was governed by four state variables: the external background (Poisson type) input to STN ((STN_{bg}) and GPe neurons (GPe_{bg}), as well as the weights of STN-GPe ($(STN - GPe)_{wt}$) and GPe-STN ($(GPe - STN)_{wt}$). We systematically adjusted these variables one by one while keeping the others constant to produce various network states. This procedure was carried out for both conditions (i.e. with and without inhibitions). The range of $4D$ parameters (network state variables) is outlined in Table 2. In addition, for each of these 4D network parameter configurations we varied the inhibitory input to the GPe neurons (to mimic striatal input) to externally alter EI balance for each network state.

Table 1: Synaptic connection properties of the STN↔GPe network model.

Synaptic Connection	No. incoming synapses/neuron	Weights	Delay (in ms)
STN→GPe	20	1.5	5
GPe→STN	40	-1.3	5
GPe→GPe	40	-.725	2

Table 2: Network Parameters used in STN↔GPe network model.

Parameter	Value	Description
STN_{bg}	[1700, 1800, 1900, 2000, 2100]	the external background (Poisson) input to STN
GPe_{bg}	[800, 900, 1200, 1300, 1400]	the external background (Poisson) input to GPe
$(STN - GPe)_{wt}$	[0.8, 1.2, 1.5, 1.6, 1.8]	the weights of STN-GPe
$(GPe - STN)_{wt}$	[-1.7, -1.5, -1.3, -1.2, -1.1]	the weights of GPe-STN

Various values of the $4D$ parameters gave rise to a variety of network activity states, distinguished by the specific oscillatory dynamics within those activities. The simulation was conducted for each network configuration spanning $1700ms$ and repeated for 25 trials. The first $700ms$ were used to allow the network to stabilize, and only the last $1000ms$ were used for further processing and analysis.

Neocortical network model: In line with our investigation of the STN-GPe network, our experimental design for the neocortical network involved a systematic adjustment of the rate of external excitatory background (Poisson) input (η) to both pyramidal and interneuron populations, as well as the fraction of excitatory synapses exclusively targeting NMDA receptors (ζ, where $\zeta \in [50 : 50 : 750]$ out of 800 synapses) within the pyramidal populations. Additionally, the ratio ("g") of inhibitory to excitatory synaptic weights was varied to control the degree of inhibition in the network. This 3D parameter set (configurations) $[g, \eta, \zeta]$ enabled us to explore the effects of these parameters on the network activity and to elucidate their role in shaping oscillation dynamics and the excitatory inhibitory balance of the network. Here we simulated 25 trials for every parameter configurations and took the average of the results. Network activity analyses were carried out in two distinct network conditions.

Base state : This condition represents the baseline or control state of the network, where the parameter "g" and ζ were set to 4 and 400, respectively.

Transition State : In this condition, we systematically varied the parameter "g" to induce transitions in the network dynamics.

Simulation tools

The dynamics of STN-GPe network and cortical network was simulated using NEST (version 3.8.0) [19]] with a simulation resolution of $0.1ms$. Runge–Kutta method with a time step of $0.1ms$ was used to solve the differential equations. The spiking activity, power spectrum, and exponent of the network were analyzed using custom code developed with the SciPy and NumPy libraries, which provide powerful tools for numerical computations and data analysis in Python 3.8.10.

Table 3: Synaptic connection properties of the neocortical network model. Here, x was varied from 50 to 750 with an increment of 50.

Connection	Incoming synapses/neuron	Weights	Delay (in ms)
$(E \rightarrow I)^{NMDA}$	x	.130	2
$(E \rightarrow I)^{AMPA}$	800-x	.149	2
$(E \rightarrow E)^{NMDA}$	x	.139	2
$(E \rightarrow E)^{AMPA}$	800-x	.159	2
$I \rightarrow E$	200	.547	2
$I \rightarrow$ I	200	.31	5

Table 4: STN and GPe Neuron Parameters (Leaky Integrate-and-Fire (LIF) Model).

Name	Value	Description
V_{reset}	-70 mV	Reset value for V_m after spike
V_{th}	-54 mV	Spike threshold
tau_{syn}^{ex}	5 ms	Time constant of excitatory synaptic conductance
tau_{syn}^{in}	10 ms	Time constant of excitatory synaptic conductance
E_{ex}	0 mV	Excitatory reversal potential
E_{in}	-80 mV	Inhibitory reversal potential
C_m	200 pF	Membrane capacitance
g_L	10 nS	Leak conductance
t_{ref}	5 ms	Duration of refractory period

Table 5: Parameters of the neocortical network model.

Name	E	I	Description
V_{reset}	-65 mV	-65 mV	Reset value for V_m after spike
V_{th}	-54 mV	-54 mV	Spike threshold
E_L	-70 mV	-70 mV	Leak reversal potential
E_{ex}	-10 mV	-10 mV	Excitatory reversal potential
E_{in}	-84 mV	-84 mV	Inhibitory reversal potential
C_m	60 pF	60 pF	Membrane capacitance
g_L	12 nS	12 nS	Leak conductance
t_{ref}	2 ms	2 ms	Duration of refractory period
$\tau_{syn}^{in}(GABA)$	5 ms	5 ms	Time constant of inhibitory synaptic conductance for GABA
$\tau_{syn}^{ex}(NMDA)$	30 ms	30 ms	Time constant of excitatory synaptic conductance for NMDA
$\tau_{syn}^{ex}(AMPA)$	3 ms	3 ms	Time constant of excitatory synaptic conductance for AMPA

Data analysis

LFP model: For network activity analysis, we recorded the excitatory and inhibitory conductances from 10 excitatory neurons (STN neurons from the STN-GPe network and pyramidal neurons from the neocortical network). These summed conductance were converted to current and treated as LFP signals [20]. Membrane conductance were recorded with a sampling rate of 1KHz.

Spectrum of population activity: The analysis of population activity spectrum (LFP) was performed using the "Welch" method. This technique involved segmenting the signal into overlapping sections, calculating the power spectrum density (PSD) estimate for each segment, and subsequently averaging these estimates to achieve a more refined spectrum. For this, we segmented the LFP signal into overlapping (50% overlap) segments of length M, where M (=256), was chosen based on the signal characteristics and the desired frequency resolution. Each segment was convolved with an "Hanning" window function to minimize spectral leakage and reduce artifacts. Subsequently, we applied the Discrete Fourier Transform (DFT), computed the squared magnitude of the DFT for each segment and averaged these across all segments to estimate the PSD. Finally, the spectrum of population activity was computed by averaging the PSD estimates across all frequency bins.

Oscillation index: To measure oscillations strength without explicitly knowing the dominant oscillation frequency we first measured the entropy of the PSD. To this end, we first normalized PSD to have unit area so that we can treat it as a probability distribution. Then we measured Shannon Entropy of the PSD derived distribution.

$$H_s = -\frac{\Sigma_k P_k log P_k}{log N} \tag{6}$$

where P_k ($\Sigma_k P_k = 1$) is the spectral power at frequency k and N is the total number of frequency bins considered. H_s is smaller when power is concentrated in a few frequencies or narrow band and maximum when power is uniformly distributed over the whole spectrum. That is, stronger the oscillations, smaller the H_s. Therefore, we defined the oscillation index (OI) as:

$$OI = 1 - H_s \tag{7}$$

Estimation of the exponent of the LFP spectrum: The decay of the spectral power of LFP like signals as a function of frequency follows a power law (i.e. $1/f^{\gamma}$). Here we used the FOOOF algorithm [21] to estimate the exponent γ (see equation 8)

$$P(f) = \frac{a}{f^{\gamma}} + b, \tag{8}$$

where $P(f)$ is the power spectral density at frequency f. γ reflects the frequency-dependent decay of aperiodic activity, with the exponent γ determining its slope. We configured the FOOOF algorithm parameters as follows: maximum number of allowed peaks in the PSD within the 50-150 Hz range (post-β range): 16; minimum peak height set to 0.01; peak threshold set to 2; peak width limits set to [0.5, 12.0] and the aperiodic mode was fixed. The lower bound of 50 Hz was chosen to minimize the impact of low-frequency oscillations in the network, which could result in error-prone aperiodic fits, while the upper bound 150 Hz was set to avoid spectral plateaus [22].

Code availability

The code to simulate the network will be uploaded on GitHub upon acceptance of the manuscript.

Results

To understand when spectral slope can be used to estimate the relative balance of excitation and inhibition (in terms of network synaptic conductances or input parameters) we simulated two different networks: STN-GPe subnetwork of the basal ganglia and a random network of mutually connected E and I neurons mimicking the

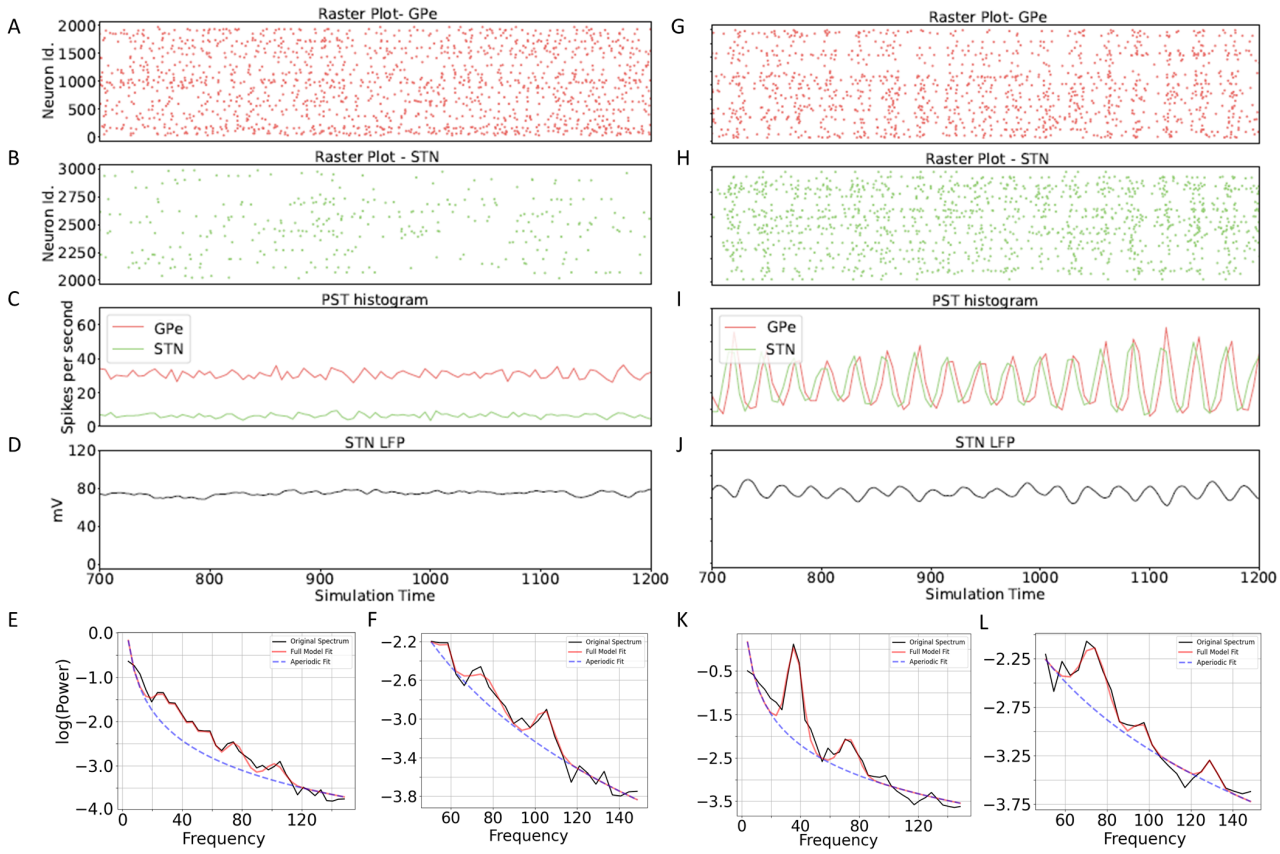

Figure 3: Computation of γ from the total conductance for network configurations corresponding to non-oscillatory (OI = 0.32 and γ = 3.49: A-F) and oscillatory conditions (OI = 0.576 and γ = 3.63: G-L). (**A**-**B**) Raster plots of GPe and STN activities, respectively. (**C**) Mean firing rate of STN and GPe population. (**D**) LFP trace corresponding to the population activity in STN. (**E**-**F**) Power spectral density of the LFP shown in the panel **D**. Red line shows the fitting of PSD using FOOOF. Blue dotted line shows the corresponding $1/f^{\gamma}$ estimate i.e. the aperiodic component. (**E**) The estimation of the aperiodic component from 5-150 HZ for γ computation. (**F**) estimate of the aperiodic component from 50-150 Hz. (**G**-**L**) Same as **A**-**F** for network configurations capable of generating oscillations in the β-range (OI = 0.576 and γ = 3.63). In **K** we show an example with β-peak which is a characteristics of PD. The sample illustration is generated from data obtained from a single trial.

neocortex. The two networks differed in the composition of neurons and recurrent connections among excitatory neurons. We systematically changed the EI-balance by varying the synaptic strengths and external input. We then tested when change in the spectral slope is consistent with the EI-balance set using network parameters (inputs and synaptic strengths).

EI-balance and spectral slope in STN-GPe network

For the STN-GPe network we systematically varied four parameters to obtain different activity states in the network: the weight from STN to GPe, the weight from GPe to STN, and the background inputs to both STN and GPe. This resulted in 625 simulations with different parameter combinations (network activity for two such combinations shown in Fig. 3 A-F and G-L). For each parameter configuration we simulated 25 trials. Thus, we obtained OI_{avg} and γ_{avg} for each of the 625 configurations over 25 trials. When we rendered the data in the space spanned by OI_{avg} and γ_{avg} we observed two distinct clusters (Fig. 4 black dots). These two clusters were mainly defined by the oscillatory dynamics in the network. Therefore, based on distribution of OI values (Fig. 4 black dots), we distinguished between a "low-oscillation regime" ($OI_{avg} <= 0.4$) and a "high-oscillation regime" ($OI_{avg} > 0.6$).

The thresholds for low-oscillation and high-oscillation regime had been chosen empirically. The high oscillatory regime was characterized by a wide range of γ_{avg} whereas in the low oscillation regime γ_{avg} was distributed over a narrow range. Based on the distribution of γ_{avg} we defined a "high exponent state" (γ_{avg} >=3) and a "low exponent state" (γ_{avg} <3).

For each of the activity regimes we varied the inhibitory inputs to the GPe neurons and thereby changed the EI balance in the network. Thus, at the synaptic level we decreased inhibition in the STN by reducing the firing rate of GPe neurons. Such a change is known to affect oscillations [15]. Here, we found that GPe inhibition also leads to a wide range of changes in the γ_{avg} depending on the network activity regime and network parameters (Fig. 4). To quantify these changes in γ_{avg} and OI_{avg} we measured the angle of the line joining the network state with and without GPe inhibition (e.g. red lines in Fig. 4A-C: arrow head mark the location in presence of GPe inhibition). An increase in γ_{avg} and OI_{avg} would results in an angle between $0^o - 90^o$ whereas a decrease in γ_{avg} and increase in OI_{avg} would results in an angle between $270^o - 0^o$ (i.e. $270^o - 360^o$).

In low OI_{avg} regime for some network configurations the change in OI_{avg} and γ_{avg} was very small. However, in general inhibiting GPe resulted in an increase in OI_{avg} while γ_{avg} could either increase or decrease as summarised in the radar plots in the inset of Fig. 4A. For another set of network parameters which rendered the network in a low OI_{avg} regime, we observed a much bigger change in both OI_{avg} and γ_{avg}. For these network configurations an increase in inhibition of GPe neurons could either increase or decrease γ_{avg} (Fig. 4C). Similar results were obtained when the network was operating in the high OI_{avg} regime. In this regime an increase in OI_{avg} was not much but γ_{avg} showed both an increase or a decrease. In all states, there was a greater tendency for a reduction in γ_{avg} (Fig. 4 D).

Thus, inhibition of GPe did not consistently reduce γ_{avg} in the STN, however, for a substantial number of cases, it reduced the exponent (Fig. 4 D) [23], as we may expect due to weaker inhibition of STN neurons by GPe. Instead, change in the spectral exponent seems to depend on both network operating regime and network parameters.

Next, we asked whether similar network states (as defined by OI_{avg} and γ_{avg}) could undergo similar transitions when GPe was inhibited, and which state variable predominantly influences the transition pattern. To this end we varied one of the network parameters and examined its effects on oscillation and exponent values (Fig. 5 A). As expected, effect of each parameter taken individually was different in the two activity regimes.

The low-oscillatory regime required high background input to the STN neurons while other parameters could take values from a large distribution (Fig. 5 A) or set in a 'sloppy' manner. High-oscillatory state, on the other hand, required weak input to STN neurons and high connectivity from STN to GPe. This is consistent with previous models [15, 17]. Upon increase in inhibitory inputs to the GPe neurons, the network could make three possible transitions: either stay in their initial low or high oscillatory state or it could make a transition from low to high oscillation state. In each of the three transitions network could take a wide range of parameters and based on a single parameter it was not possible to predict what kind of transition would be observed (Fig. 5 B).

Finally, we looked at the change in γ_{avg} when network made a transition from low to high oscillation regime. In these simulations γ_{avg} either increased or decreased from the starting value. Once again, individual parameters were drawn from a larger distribution for these transitions. Thus, individual parameters cannot help in predicting whether the network will show an increase or a decrease in γ_{avg} when oscillations increased (Fig. 5 C). However, stronger synaptic weights from the STN to GPe and from GPe to STN were associated with increased exponent values during the transition from low to high oscillations [24].

To better understand the relationship between EI balance and the exponent of the spectrum of population activity

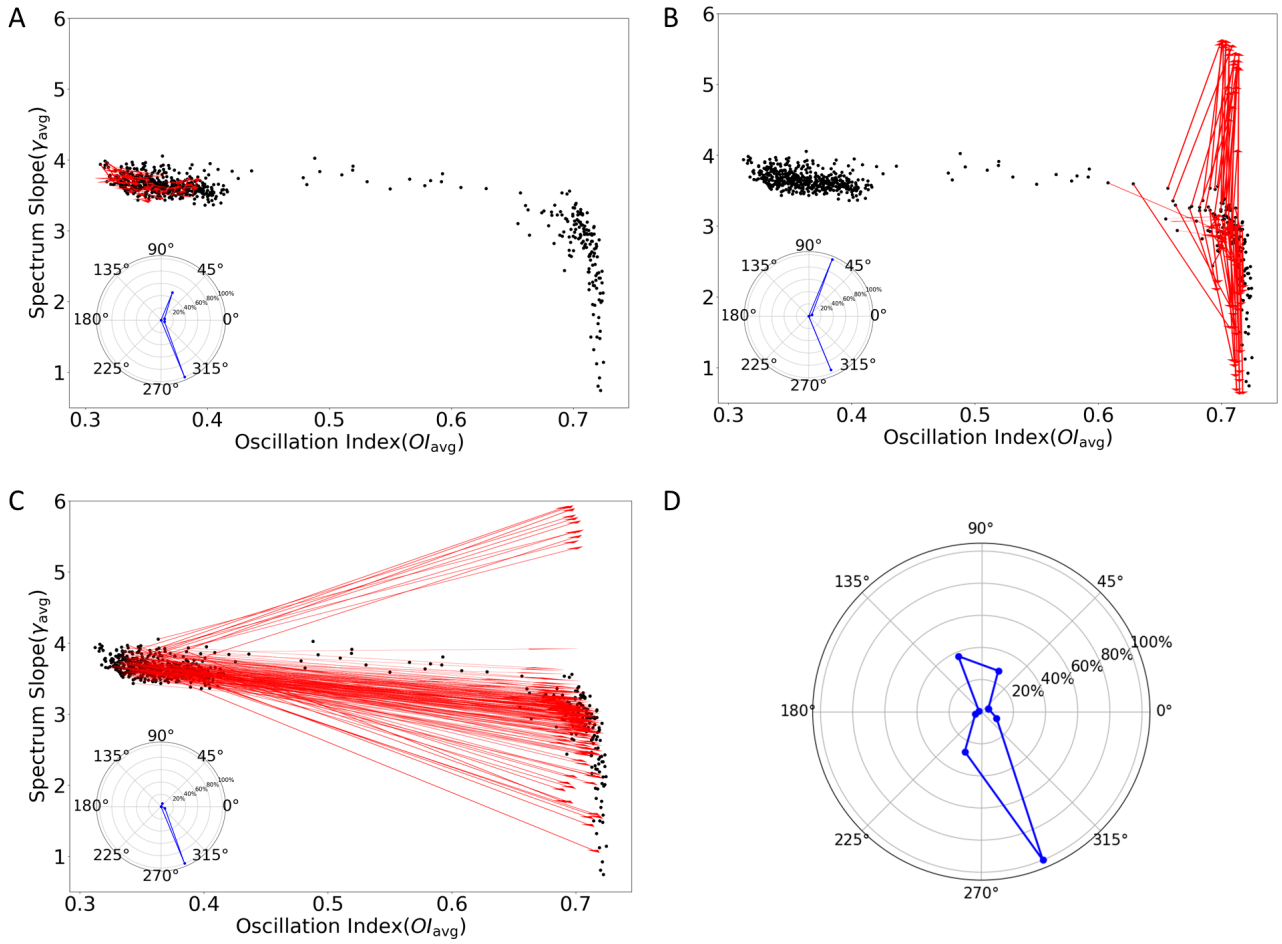

Figure 4: **Change in STN-GPe network states when GPe was inhibited.** (**A**) Black dots indicate the state of the STN-GPe network as defined by γ_{avg} and OI_{avg}. Each black dot corresponds to one of 625 configurations of the network parameters. Red arrows heads indicate the change in the network state when GPe was inhibited. Here red arrows show only the transitions for network configurations that resulted in a non-oscillatory regime and GPe inhibition did not induced a activity regime change. Inset: distribution of directions of red arrows. (**B**) Same as in panel A but red arrows here indicate inhibition induced state change for networks that were operating in a high oscillation regime. (**C**) Same as in panel A but red arrows here indicate inhibition induced state change for networks that were initially operating in a low oscillation regime. (**D**) Histogram of the transition directions of $[OI_{avg}, \gamma_{avg}]$ occurring with 600 Hz inhibitory input in the network under basal state for all configurations.

we mean excitatory and inhibitory conductances. Again, as we increased the inhibition of GPe, oscillations and γ_{avg} could increase or decrease. To quantify this change, we defined four possible transitions, i.e. both γ and OI can increase or decrease independently. We expected that an increase in inhibitory conductance would be associated with an increase in γ_{avg} and oscillations would increase (i.e. arrows pointing north, north-east). However, when we rendered the data as a function of E and I conductance we did not find a clear relationship between E-I conductance ratio and direction of the arrows (see Fig. 6). For the same average excitatory-inhibitory conductance we could see both an increase and decrease in γ_{avg}, irrespective of whether the starting state of the network was oscillatory or non-oscillatory (compare Fig. 6,A,B). The results were the same when restricted the analysis to cases when increased inhibition of GPe did not result in a change in the activity regime.

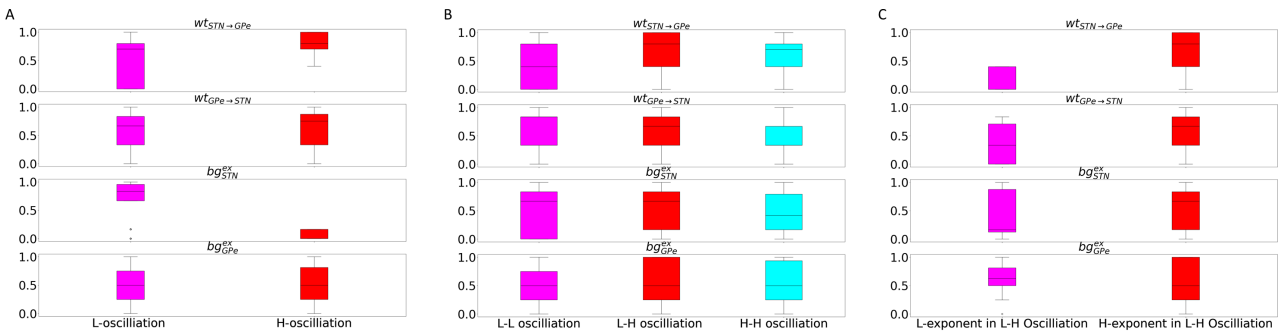

Figure 5: **Effect of network parameters in shaping the network state and its transition when GPe is inhibited.** For a meaningful comparison we normalized each parameter using the formula $\frac{x-\min(x)}{\max(x)-\min(x)}$, where x comprises $(STN-GPe)_{wt}$ or $wt_{STN-GPe}$, $(GPe-STN)_{wt}$ or $wt_{GPe-STN}$, STN_{bg} or bg^{ex}_{STN}, GPe_{bg} or bg^{ex}_{GPe}. (**A**) Distribution of four parameters when the network was either in low-oscillation or high-oscillation regimes. This refers to the states marked with black dots in the Fig. 4 A-C. (**B**) The distribution of parameters during various types of inhibition-induced transitions, namely low to low, low to high, and high to high oscillation zones. (**C**) Same as in **B** Distribution of parameters when GPe inhibition resulted in transition to a smaller and higher exponent value from their baseline. This panel was made using data shown in Fig. 4C.

Neocortical network model

A lack of clear relationship between slope of population activity spectrum excitation-inhibition balance could be a property specific to the STN-GPe network. Therefore, next we turned to a model of neocortical network in which both excitatory and inhibitory connection are mutually connected with a fixed connection probability (see Methods).

In this model we systematically varied the external input, the ratio of recurrent inhibition and excitation, and the ratio of NMDA and AMPA components in excitatory synapses. These parameters rendered the network with different activity states characterized by weak and strong oscillations (also synchrony). For each combination of network parameters we estimated the strength of oscillations (OI_{avg}) and exponent of the spectral slope (γ_{avg}). As is already known, oscillations increased with the strength of external inputs (Fig. 7 A). By contrast, effect of increasing inhibition was contingent on the external input. When the network was driven by strong external input, increasing inhibition tended to reduce oscillations (Fig. 7 A). Increasing the NMDA component in excitatory synapses increased oscillations without affecting the dependence of oscillations on g and η.

Unlike the oscillations, the exponent of spectral slope (γ_{avg}) did not show any pattern with respect to g and η (Fig. 7 B). An increase in the NMDA component made the synapses slower. Therefore, increase in the NMDA component resulted in an increase in the spectral slope (compare rows of the Fig. 7 B).

To further illustrate that γ_{avg} is not directly related to EI balance in terms of synaptic conductances we compared how γ_{avg} and OI_{avg} change when synaptic inhibition was increased from a baseline state. For the baseline state we chose $g = 4$. We then increased g and rendered the network state in the space spanned by γ_{avg} and OI_{avg} (Fig. 8 A-B). Because we increased g we expected γ_{avg} to increase. That is, we expect the arrows in the Fig. 8 A,B to point north or north east direction. However, as is evident in the Fig. 8 A,B increase in g could both increase or decrease γ_{avg} (see summary in the Fig. 8 C).

Thus, our simulations show that in both STN-GPe network and simplified model of cortical networks slope of the population activity spectrum is not changing in a manner consistent with the network parameters (synaptic weights and inputs).

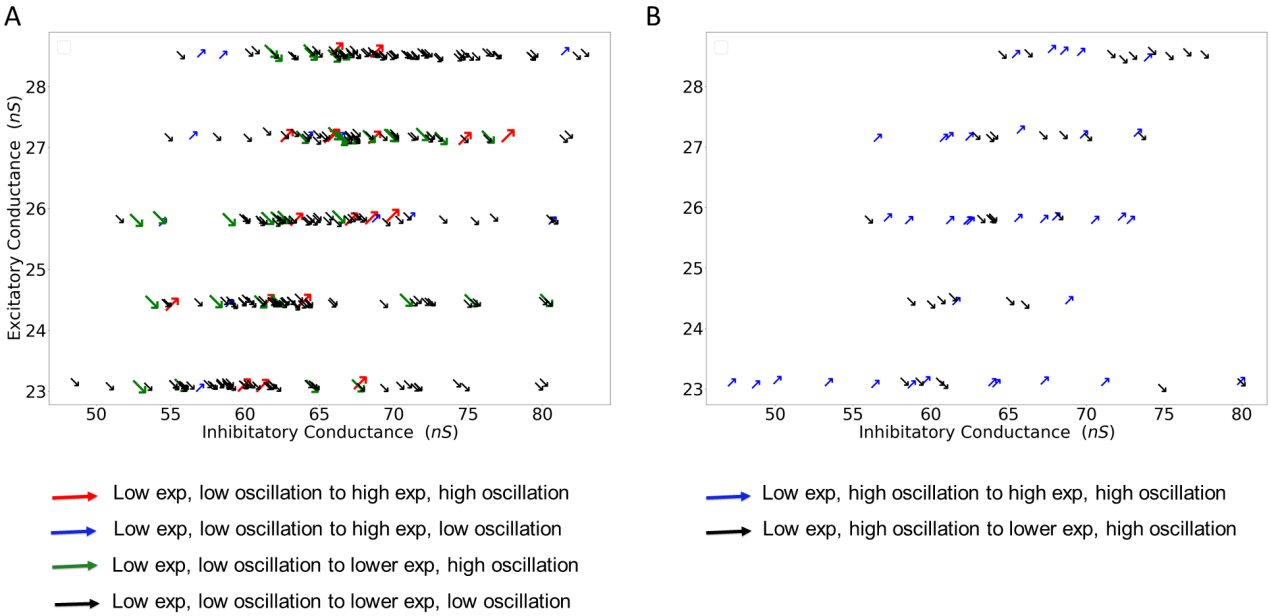

Figure 6: **Relationship between excitatory and inhibitory conductance and the slope of the population activity spectrum.** Here we re-render the data shown in Fig. 4. Inhibition induced changes in the network state were reduced to four possibilities: increase or decrease in oscillations and increase or decrease in spectral slope. Thus, the network could move in four possible directions. These directions are rendered as arrows in the two panels as a function of average excitatory (y-axis) and inhibitory conductance (x-axis). **(A)** Inhibitory induced change in the network state when the network was operating in non-oscillatory regime. **(B)** Same as in panel A but here the network was operating in oscillatory regime. In both cased we did not find a clear trend between direction of the arrows and average excitation-inhibition.

Discussion

Balance of excitation-inhibition is an important descriptor of the dynamics [2, 1, 3], and function of a network [4, 25]. Gao et al. [12] have suggested that relative EI-balance information can be obtained by comparing the slope of the spectrum of population activity such as EEG/MEG. This has renewed an interest in measuring the slope of the LFP/EEG/MEG spectrum in various behavioral and disease states. Essentially what Gao et al. [12] are suggesting is that there is a systematic relationship between the spectral slope and underlying network parameters which determine the EI balance in some way. Here we set out to test this idea in two different network models where we knew the ground truth in terms of the conductance of excitatory and inhibitory synapses. We found that only in some cases a change the spectral slope was consistent with the change in the EI-balance as determined by our network parameters.

In general, in our simulations it was not possible to say that a state with higher γ_{avg} was generated by a network with stronger inhibitory conductances (due to inputs or synaptic weights) than the other state with a smaller γ_{avg}. In our model, we varied the network parameters in a range wide enough to produce different activity regimes (e.g. oscillatory or non-oscillatory). However, even g has no clear relationship with the spectral slope (Fig. 7). Thus, in both network models we did not find any systematic relationship between spectral slope and network parameters. This is a rather surprising observation and suggests that changes in the spectral slope cannot be always interpreted in terms of putative changes in the network parameters.

When we consider an unconnected population of neurons driven by excitatory and inhibitory spikes, indeed spectral slope is determined by the ratio of excitatory and inhibitory inputs. However, in a recurrent network, as we change the excitatory drive or recurrent inhibition, a recurrent network responds with a change in the firing rates of both

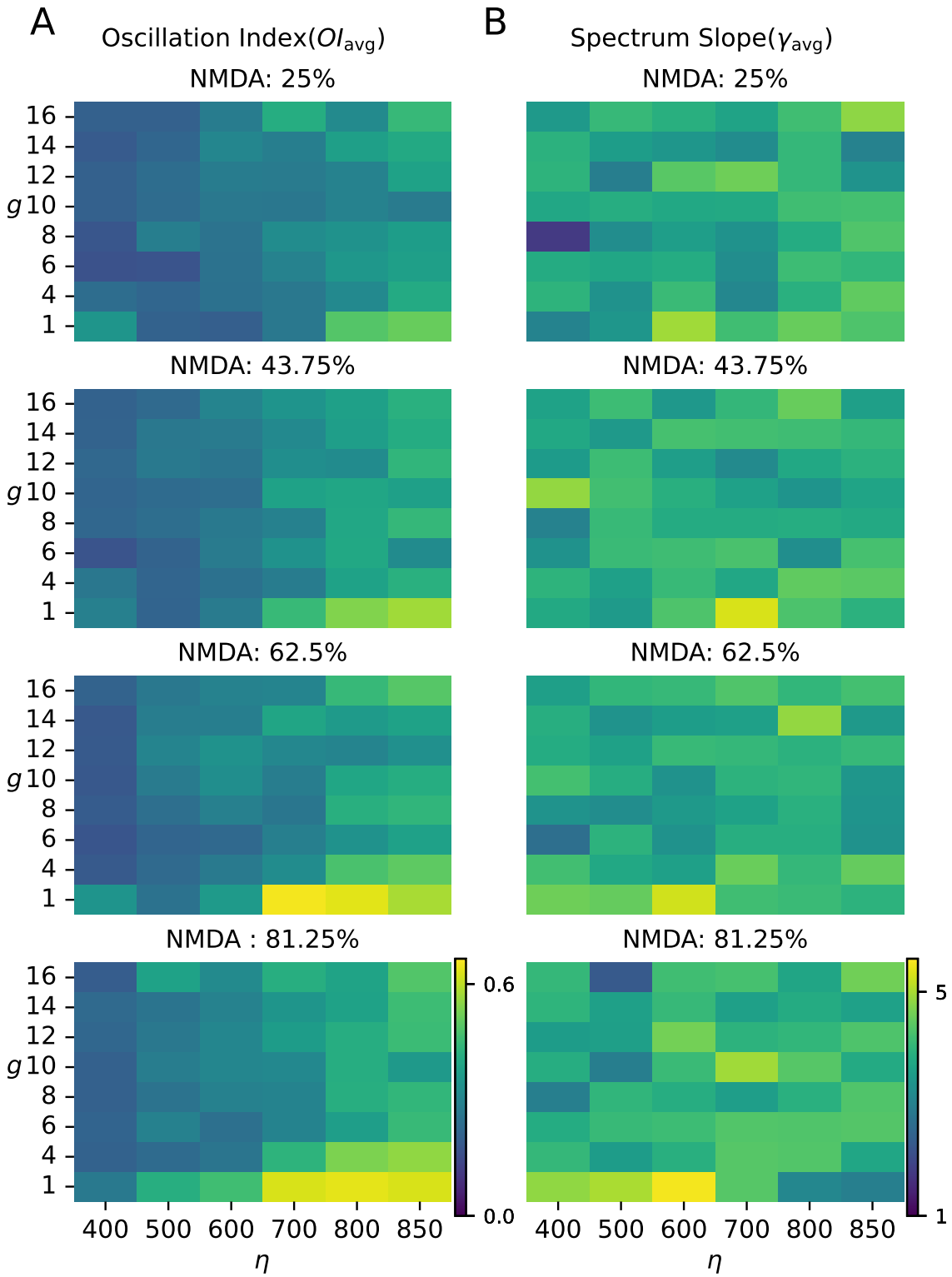

Figure 7: **Network oscillations and slope of the spectrum of population activity in a model of neocortical network.** (A) Oscillation (OI_{avg}) and (B) slope of the spectrum (γ_{avg}) as a function of ratio of recurrent inhibition and excitation (g) and external input (η).Each row represents the network with specific ratio of NMDA and AMPA current in excitatory synapses.

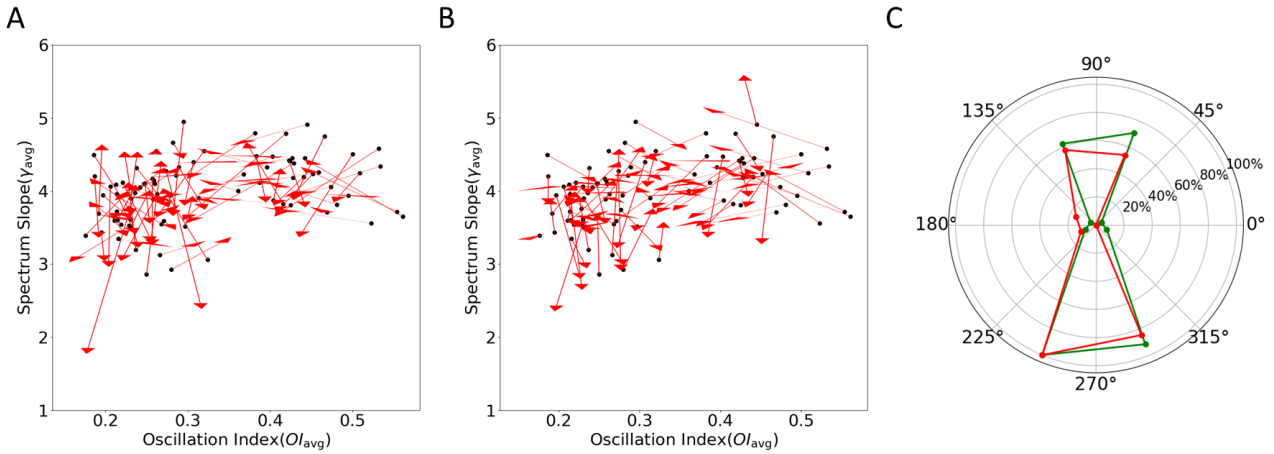

Figure 8: **Increase in synaptic inhibition does not imply an increase in γ_{avg}.** (**A**) The starting points of the arrows show the network state (OI_{avg}, γ_{avg}) for $g = 4$ and arrows heads indicate the network state for $g = 8$. (**B**) Same as in the panel A but now arrows heads indicate the network state for $g = 12$. (**C**) Distribution of the directions of the arrows shown in panels A and B. Red trace: distribution for change in network state when g changes from 4 to 8. Green trace: distribution for change in network state when g changes from 4 to 12.

excitatory and inhibitory neurons – the exact change the firing rates depends on the network configuration (balanced or inhibition stabilized mode) and strength of synapses [1, 26, 27]. Therefore, it is not a surprise that a change in the spectral slope does not indicate a change in excitatory and/or inhibitory input rates or synaptic strengths.

Admittedly, the network models we have considered are highly simplified (e.g. they consist of homogeneous neuron population connected with same synaptic strengths). In particular, such network models do not generate biologically realistic spectrum of population activity – in the sense that such models often produce a single frequency oscillations. Furthermore, we have used point neurons in the model and therefore, our model of LFP cannot capture the full nuances of the LFP (or our such measures of population activity) [28]. Similarly, as we have used point neurons we could only generate LFP by summing synaptic currents. It is not feasible to use morphologically realistic neuron model in network simulations. However, the literature suggests that networks with morphologically realistic neurons model also produced similar dynamics [29] and neuron shape by itself does not alter the shape of population activity waveforms [30]. However, if we cannot find a relationship between network parameters and spectral slope even in a simplified model like ours, it is unlikely that a relationship will show up in more biological models. Spectral slope and EI balance are complex concepts. While both are determined by network parameters and network dynamics, they perhaps represent different kinds of coarsegraining and therefore they are not related directly.

Irrespective of the simplicity of our models, the message is clear that EI balance is a very complex concept and it emerges in the network through interactions of excitatory and inhibitory neurons given synaptic strengths, inputs and connectivity. Therefore, even if we notice a change in the synaptic strengths we cannot predict which way the EI balance (and spectral slope) would shift or the network will restore the balance. That is, *a priori* we should not assume that an increase in the spectral slope implied an increase in the inhibition (or NMDA component in excitatory synapses).

Given the importance of estimating EI-balance from population activity spectrum, it is crucial that spectral slopes are measured experimentally under different behavioral states and stimulation paradigms to develop a more correct interpretation. We also note that even if it is not possible to relate the spectral slope to network parameters (and

EI-balance), as long as the measure forms a basis for the classification of different patients groups the measure remains valuable.

Acknowledgement

We thank Dr. Pascal Helson and Archishman Biswas for helpful suggestions and feedback on the text.

References

[1] Van Vreeswijk, C. & Sompolinsky, H. Chaos in neuronal networks with balanced excitatory and inhibitory activity. *Science* **274**, 1724–1726 (1996).

[2] Brunel, N. Dynamics of sparsely connected networks of excitatory and inhibitory spiking neurons. *Journal of computational neuroscience* **8**, 183–208 (2000).

[3] Kumar, A., Schrader, S., Aertsen, A. & Rotter, S. The high-conductance state of cortical networks. *Neural computation* **20**, 1–43 (2008).

[4] Hennequin, G., Vogels, T. P. & Gerstner, W. Optimal control of transient dynamics in balanced networks supports generation of complex movements. *Neuron* **82**, 1394–1406 (2014).

[5] Rajan, K., Abbott, L. & Sompolinsky, H. Stimulus-dependent suppression of chaos in recurrent neural networks. *Physical Review E—Statistical, Nonlinear, and Soft Matter Physics* **82**, 011903 (2010).

[6] Guo, L. & Kumar, A. Role of interneuron subtypes in controlling trial-by-trial output variability in the neocortex. *Communications Biology* **6**, 874 (2023).

[7] Li, Q. & Pehlevan, C. Minimax dynamics of optimally balanced spiking networks of excitatory and inhibitory neurons. *Advances in neural information processing systems* **33**, 4894–4904 (2020).

[8] Hennequin, G., Agnes, E. J. & Vogels, T. P. Inhibitory plasticity: balance, control, and codependence. *Annual review of neuroscience* **40**, 557–579 (2017).

[9] Kremkow, J., Aertsen, A. & Kumar, A. Gating of signal propagation in spiking neural networks by balanced and correlated excitation and inhibition. *Journal of neuroscience* **30**, 15760–15768 (2010).

[10] Cafaro, J. & Rieke, F. Noise correlations improve response fidelity and stimulus encoding. *Nature* **468**, 964–967 (2010).

[11] Tatti, R., Haley, M. S., Swanson, O. K., Tselha, T. & Maffei, A. Neurophysiology and regulation of the balance between excitation and inhibition in neocortical circuits. *Biological psychiatry* **81**, 821–831 (2017).

[12] Gao, R., Peterson, E. J. & Voytek, B. Inferring synaptic excitation/inhibition balance from field potentials. *Neuroimage* **158**, 70–78 (2017).

[13] Einevoll, G. T., Kayser, C., Logothetis, N. K. & Panzeri, S. Modelling and analysis of local field potentials for studying the function of cortical circuits. *Nature Reviews Neuroscience* **14**, 770–785 (2013).

[14] El Boustani, S. & Destexhe, A. A master equation formalism for macroscopic modeling of asynchronous irregular activity states. *Neural computation* **21**, 46–100 (2009).

[15] Kumar, A., Cardanobile, S., Rotter, S. & Aertsen, A. The role of inhibition in generating and controlling parkinson's disease oscillations in the basal ganglia. *Frontiers in systems neuroscience* **5**, 86 (2011).

[16] Bahuguna, J., Sahasranamam, A. & Kumar, A. Uncoupling the roles of firing rates and spike bursts in shaping the stn-gpe beta band oscillations. *PLoS computational biology* **16**, e1007748 (2020).

[17] Holgado, A. J. N., Terry, J. R. & Bogacz, R. Conditions for the generation of beta oscillations in the subthalamic nucleus–globus pallidus network. *Journal of Neuroscience* **30**, 12340–12352 (2010).

[18] Chakravarty, K. *et al.* Transient response of basal ganglia network in healthy and low-dopamine state. *eNeuro* **9** (2022). URL `https://www.eneuro.org/content/9/2/ENEURO.0376-21.2022`. `https://www.eneuro.org/content/9/2/ENEURO.0376-21.2022.full.pdf`.

[19] Gewaltig, M.-O. & Diesmann, M. Nest (neural simulation tool). *Scholarpedia* **2**, 1430 (2007).

[20] Mazzoni, A. *et al.* Computing the local field potential (lfp) from integrate-and-fire network models. *PLoS computational biology* **11**, e1004584 (2015).

[21] Donoghue, T. *et al.* Parameterizing neural power spectra into periodic and aperiodic components. *Nature neuroscience* **23**, 1655–1665 (2020).

[22] Gerster, M. *et al.* Separating neural oscillations from aperiodic 1/f activity: challenges and recommendations. *Neuroinformatics* **20**, 991–1012 (2022).

[23] Wiest, C. *et al.* The aperiodic exponent of subthalamic field potentials reflects excitation/inhibition balance in parkinsonism. *elife* **12**, e82467 (2023).

[24] Lindahl, M. & Kotaleski, J. H. Untangling basal ganglia network dynamics and function: Role of dopamine depletion and inhibition investigated in a spiking network model. *eneuro* **3** (2016).

[25] Denève, S. & Machens, C. K. Efficient codes and balanced networks. *Nature neuroscience* **19**, 375–382 (2016).

[26] Murphy, B. K. & Miller, K. D. Balanced amplification: a new mechanism of selective amplification of neural activity patterns. *Neuron* **61**, 635–648 (2009).

[27] Sadeh, S. & Clopath, C. Inhibitory stabilization and cortical computation. *Nature Reviews Neuroscience* **22**, 21–37 (2021).

[28] Halnes, G. *et al.* *Electric brain signals: foundations and applications of biophysical modeling* (Cambridge University Press, 2024).

[29] Billeh, Y. N. *et al.* Systematic integration of structural and functional data into multi-scale models of mouse primary visual cortex. *Neuron* **106**, 388–403 (2020).

[30] Lindén, H. *et al.* Modeling the spatial reach of the lfp. *Neuron* **72**, 859–872 (2011).